View metadata, citation and similar papers at core.ac.uk

brought to you by CORE

provided by Kyoto University Research Information Repository

KURENAI
Kyoto University Research Information Repository

KYOTO UNIVERSITY

Title	Influence of Electrolyte Composition on the Electrochemical Reaction Mechanism of Bismuth Fluoride Electrode in Fluoride Shuttle Battery
Author(s)	Konishi, Hiroaki; Minato, Taketoshi; Abe, Takeshi; Ogumi, Zempachi
Citation	Journal of Physical Chemistry C (2019), 123(16): 10246-10252
Issue Date	2019-4-25
URL	http://hdl.handle.net/2433/243871
Right	This document is the Accepted Manuscript version of a Published Work that appeared in final form in 'Journal of Physical Chemistry C'. copyright © American Chemical Society after peer review and technical editing by the publisher. To access the final edited and published work see https://doi.org/10.1021/acs.jpcc.9b00455.; The full-text file will be made open to the public on 17 April 2020 in accordance with publisher's 'Terms and Conditions for Self-Archiving'; This is not the published version. Please cite only the published version. この論文は出版社版でありません。引用の際には出版社版をご確認ご利用ください。
Type	Journal Article
Textversion	author

Kyoto University

Influence of Electrolyte Composition on the Electrochemical Reaction Mechanism of Bismuth Fluoride Electrode in Fluoride Shuttle Battery

Hiroaki Konishi,[a, *] Taketoshi Minato,[b, *] Takeshi Abe,[c, *] and Zempachi Ogumi,[a]

[a] Office of Society-Academia Collaboration for Innovation, Kyoto University, Gokasho, Uji, Kyoto 611-0011, Japan

[b] Office of Society-Academia Collaboration for Innovation, Kyoto University, Katsura, Nishikyo, Kyoto 615-8510, Japan

[c] Graduate School of Global Environmental Studies, Kyoto University, Katsura, Nishikyo, Kyoto 615-8510, Japan

The Journal of Physical Chemistry C, **123**, 10246–10252 (2019).

* **Corresponding author**

Hiroaki Konishi

E-mail: hiroaki.konishi.yj@hitachi.com

Tel: +81 294 52 5111

Taketoshi Minato

E-mail: minato.taketoshi.5x@kyoto-u.ac.jp

Tel: +81 75 383 7220

Takeshi Abe

E-mail: abe@elech.kuic.kyoto-u.ac.jp

Tel: +81 75 383 2487

ORCID

Hiroaki Konishi: 0000-0002-2787-6366

Taketoshi Minato: 0000-0002-5443-1709

Present address

Hiroaki Konishi

Research & Development Group, Hitachi Ltd.

Hitachi, Ibaraki 319-1292, Japan

E-mail: hiroaki.konishi.yj@hitachi.com

Abstract

The fluoride shuttle battery (FSB) is a promising next-generation battery candidate. In the FSB, a metal fluoride and organic solvent containing supporting electrolyte salt and anion acceptor were used as active material and electrolyte. In this study, using bis[2-(2-methoxyethoxy)ethyl] ether (tetraglyme: G4) containing cesium fluoride (CsF; 0.45 mol dm^{-3} or saturated) and triphenylboroxine (TPhBX; 0.50 mol dm^{-3}) as electrolyte (CsF(0.45)-TPhBX(0.50)-G4 and CsF(sat.)-TPhBX(0.50)-G4), the electrochemical performance of bismuth fluoride (BiF_3) was assessed. Although the discharge and charge reactions of BiF_3 electrode proceeded in both electrolytes, the cycling performance of BiF_3 electrode in CsF(0.45)-TPhBX(0.50)-G4 was poorer than that in CsF(sat.)-TPhBX(0.50)-G4. The cause of differences in the electrochemical properties was investigated using atomic absorption spectrometry (AAS), X-ray photoelectron spectroscopy (XPS), and cross-sectional scanning electron microscopy (SEM)/ energy dispersive X-ray spectroscopy (EDX). The AAS results indicate that the poor cycling performance with CsF(0.45)-TPhBX(0.50)-G4 was due to dissolution of active material during charging. The XPS and cross-sectional SEM/EDX results indicate that the formation state of Bi and progress of electrolyte decomposition during discharging were affected by CsF/TPhBX ratio in the electrolyte.

Introduction

Lithium-ion batteries (LIBs) are widely used as power sources for electronic devices. [1–3] Improvements in device performances necessitate high-energy-density batteries that surpass existing LIBs. Hence, many next-generation high-energy batteries have been developed. [4–7] Recently, Reddy et al. proposed a battery which utilizes anion migration to perform the electrochemical reaction, [8] and several groups have been developing these batteries now. [9–14] We recently developed a liquid-based fluoride shuttle battery (FSB). [15–18] For the FSB, a metal fluoride (MF_x; M: metal) was used as an active material, and the electrochemical reaction of the active material proceeded according to equations (i) and (ii):

(Discharge process) $MF_x + xe^- \rightarrow M + xF^-$ (i)

(Charge process) $M + xF^- \rightarrow MF_x + xe^-$ (ii)

To promote the electrochemical reaction for the FSB within a wide potential range, the electrolyte consisted of organic solvent and supporting electrolyte salt. However, the supporting electrolyte salt, cesium fluoride (CsF), barely dissolved in the organic solvent. [15] It was reported that an anion acceptor (AA) was effective in attracting fluoride ions and increasing the fluoride solubility. [19–23] In our previous study, the effect of AA additive on

the solubility of CsF was investigated, and the results indicated that this was effective in increasing the solubility. [15–18] A bismuth fluoride (BiF_3) was selected as an active material due to its high theoretical capacity (302 mAh g^{-1}). [24–29] Using an electrolyte comprising bis[2-(2-methoxyethoxy)ethyl] ether (tetraglyme: G4) containing CsF and an AA such as fluorobis(2,4,6-trimethylphenyl)borane (FBTMPhB), triphenylboroxine (TPhBX), or triphenylborane (TPhB), the discharge and charge reactions of BiF_3 electrode proceeded successfully; however, the discharge and charge capacities of BiF_3 decreased drastically during cycling. [15] We investigated the reason for the poor cycling performance and found that, in addition to the BiF_3 formation ($Bi + 3F^- \rightarrow BiF_3 + 3e^-$), Bi dissolved ($Bi \rightarrow Bi^{3+} + 3e^-$) during charging. This meant that active material was lost during charging; thus, the discharge and charge capacities decreased. To suppress the Bi dissolution during charging, the molar ration of CsF/FBTMPhB in the electrolyte was controlled. Increasing in the CsF/FBTMPhB ratio effectively improved the cycling performance; [16] however, the detailed mechanism has not yet been clarified.

In this study, the influence of the CsF/AA ratio on the cycling performance of BiF_3 electrode was confirmed using TPhBX as an AA. The influence of the CsF/AA ratio on the cycling performance of BiF_3 electrode was investigated using electrolytes containing different CsF/TPhBX ratios. In order to clarify the difference in the

electrochemical reaction mechanism in each electrolyte, the electronic state of Bi, amount of dissolved Bi, and particle configuration of active material were investigated using X-ray photoelectron spectroscopy (XPS), atomic absorption spectrometry (AAS), and cross-sectional scanning electron microscopy (SEM)/ energy dispersive X-ray spectroscopy (EDX).

2. Experimental

2.1. Electrolyte preparation

As for the electrolyte, the G4 (KISHIDA CHEMICAL Co., Ltd.) containing 0.45 mol dm^{-3} or saturated (0.51 mol dm^{-3}) CsF (Tokyo Chemical Industry Co., Ltd) and 0.50 mol dm^{-3} TPhBX (Tokyo Chemical Industry Co., Ltd.) was prepared in a glove box with high-purity Ar. The G4 containing 0.45 mol dm^{-3} CsF and 0.50 mol dm^{-3} TPhBX was labeled CsF(0.45)-TPhBX(0.50)-G4. The G4 containing saturated CsF and 0.50 mol dm^{-3} TPhBX was labeled CsF(sat.)-TPhBX(0.50)-G4.

2.2. Electrochemical window of the electrolyte

To evaluate the electrochemical windows of CsF(0.45)-TPhBX(0.50)-G4 and CsF(sat.)-TPhBX(0.50)-G4, cyclic voltammetry (CV) was conducted with a three-

electrode electrochemical cell (EC FRONTIER CO., Ltd. VB7) comprising a platinum-foil as the working electrode, a platinum-mesh as the counter electrode, and a silver rod immersed in acetonitrile containing 0.10 mol dm^{-3} silver nitrate and 0.10 mol dm^{-3} tetraethylammonium perchlorate as the reference electrode (0.587 V vs. standard hydrogen electrode). [30] The electrochemical cell was assembled in a glove box. CV was conducted at room temperature using a multipotentiostat (Biologic VMP-300) between –3.0 and 0 V (vs. ref.) at a sweep rate of 0.1 mV s^{-1}.

2.3. Electrochemical performance of the BiF_3

A BiF_3 (Fluorochem Ltd.) was used as the active material. BiF_3, acetylene black, and polyvinylidene difluoride were mixed in the ratio 60: 25: 15 wt%, and N-methyl-2-pyrrolidone (NMP) was subsequently added. The resulting slurry was coated on an aluminum current collector, and the NMP was evaporated at 110°C. The discharge and charge capacities of the BiF_3 electrodes were determined with a three-electrode electrochemical cell comprising a BiF_3 electrode as the working electrode, a platinum-mesh as the counter electrode, and a silver rod immersed in acetonitrile containing 0.10 mol dm^{-3} silver nitrate and 0.10 mol dm^{-3} tetraethylammonium perchlorate as the reference electrode. The electrochemical cell was assembled in a glove box filled with

high-purity Ar. Charge and discharge measurements were conducted using a multipotentiostat (Biologic VMP-300) between –1.2/–2.0 and –0.2 V (vs. ref.) at 0.025C (1C = 302 mA g^{-1}) at room temperature in a glove box. The specific capacity was calculated by dividing the capacity by the weight of the active material (BiF_3).

2.4. Electronic state of Bi in the BiF_3 electrode during discharging and charging

The electronic state of Bi in the BiF_3 electrode was analyzed by XPS (Ulvac Phi Quantera SXM^{TM}) using Al Kα X-ray radiation under ultra-high vacuum conditions. After the BiF_3 electrodes were discharged and charged, they were sequentially washed with G4 and dimethylcarbonate (DMC) to remove residual electrolyte. The BiF_3 electrodes were then transferred to an XPS chamber without exposure to air using transfer vessels filled with high-purity Ar. XPS spectra of BiF_3 electrodes were measured after Ar^+ sputtering (Ar^+ energy: 2 keV, ion current 3 μA, and time: 16 min). The binding energy was calibrated based on the Bi $4f_{7/2}$ peak of Bi metal at 156.9 eV, and the spectral intensity was normalized based on the peak area of the Bi $4f_{5/2}$ peaks.

2.5. Amount of dissolved Bi in the electrolyte

The amount of dissolved Bi in the electrolyte was analyzed by AAS (Hitachi

ZA3000). The amounts of dissolved Bi in the electrolyte in the fully discharged and charged states during the first cycle were determined.

2.6. Cross-sectional observation of BiF_3 electrode during discharging

Cross-sections of the BiF_3 electrodes in the pristine and partially discharged states (151 mAh g^{-1}) were observed by SEM (JEOL JSM7100F). After the BiF_3 electrodes were discharged, they were sequentially washed with G4 and DMC to remove residual electrolyte. The BiF_3 electrodes were then cut using an ion-milling system (Hitachi IM4000) for examination by SEM. The Bi, F, and Cs distributions in the particle were determined by EDX (Thermo Scientific Noran System Seven). The incident electron beam energies were 5 keV (Bi, F, and O) and 7 keV (Cs). All preparation and measurement processes were performed without the exposing the sample to air.

3. Results and Discussion

3.1. Electrochemical window of the electrolyte

To evaluate the effect of CsF/TPhBX ratio in the electrolyte on the electrochemical window, CVs were performed in CsF(0.45)-TPhBX(0.50)-G4 and CsF(sat.)-TPhBX(0.50)-G4 (Figure 1). Oxidation peaks were hardly observed in both

electrolytes. Conversely, reduction peak in CsF(sat.)-TPhBX(0.50)-G4 was observed at lower potential than that in CsF(0.45)-TPhBX(0.50)-G4. This indicates that the electrochemical window was expanded by the increase in the CsF/TPhBX ratio.

3.2. Electrochemical performance of BiF_3 in each electrolyte

To evaluate the effect of CsF/TPhBX ratio in the electrolyte on the electrochemical performance of BiF_3 electrode, charge and discharge measurements were performed in each electrolyte. The discharge and charge curves of BiF_3 electrodes in both electrolytes are shown in Figure 2. As reported previously, when BiF_3 electrode was cycled in CsF(0.45)-TPhBX(0.50)-G4, the first, second, and third discharge/charge capacities of BiF_3 were 318/130, 38/46, and 7/14 mAh g^{-1} (Inset in Figure 2). [18] When the BiF_3 electrode was discharged to –1.2 V using CsF(sat.)-TPhBX(0.50)-G4, the discharge reaction hardly proceeded; therefore, the discharge cut-off potential was changed to –2.0 V when using CsF(sat.)-TPhBX(0.50)-G4. When BiF_3 electrode was cycled in CsF(sat.)-TPhBX(0.50)-G4, the first, second, and third discharge/charge capacities of BiF_3 were 319/82, 94/89, and 98/89 mAh g^{-1}. A large irreversible capacity was observed for the first cycle, but there was minimal irreversible capacity for both the second and third cycles. Although the first reversible capacity of BiF_3 with CsF(sat.)-

TPhBX(0.50)-G4 was lower than that with CsF(0.45)-TPhBX(0.50)-G4, the former exhibited a higher cycling performance than the latter.

3.3. Electronic state of Bi in BiF_3 electrode during discharging and charging in each electrolyte

To confirm the progress of discharge and charge reactions for BiF_3 electrode in each electrolyte, the electronic state of Bi in the BiF_3 electrode during the initial discharging and charging was evaluated using XPS. Bi 4f XPS spectra of the BiF_3 electrode during the initial discharging and charging in each electrolyte are shown in Figure 3.

Firstly, the electronic state of Bi in the BiF_3 electrode prepared using CsF(0.45)-TPhBX(0.50)-G4 was explored. According to Figure 3(a), in the pristine state, two peaks were observed at 160.5 and 165.8 eV, which were assigned as Bi $4f_{7/2}$ and $4f_{5/2}$ peaks of Bi^{3+} in BiF_3. [31, 32] From the pristine to the partially discharged state, to the fully discharged state, the peak intensity observed at 160.5 and 165.8 eV decreased, while new peaks at 156.9 and 162.2 eV appeared, and the peak intensity increased. Those peaks are indexed to Bi $4f_{7/2}$ and $4f_{5/2}$ of Bi metal. [31, 32] This indicates that the discharge reaction ($BiF_3 + 3e^- \rightarrow Bi + 3F^-$) proceeds in CsF(0.45)-TPhBX(0.50)-G4. From the fully discharged to fully

charged states, the peak intensity assigned to Bi metal decreased while that assigned to BiF_3 increased. This indicates that the charging reaction ($Bi + 3F^- \rightarrow BiF_3 + 3e^-$) proceeds in CsF(0.45)-TPhBX(0.50)-G4.

Secondly, the electronic state of Bi in the BiF_3 electrode prepared using CsF(sat.)-TPhBX(0.50)-G4 was explored. According to Figure 3(b), from the pristine to the partially discharged state, to the fully discharged state, the peak intensity assigned to Bi $4f_{7/2}$ and $4f_{5/2}$ of BiF_3 (160.5 and 165.8 eV) decreased, while new peaks assigned to Bi $4f_{7/2}$ and $4f_{5/2}$ of Bi metal (156.9 and 162.2 eV) and Cs $4p_{3/2}$ of Cs (159.6 eV) appeared, [33] and the peak intensity increased. This indicates that the discharge reaction ($BiF_3 + 3e^- \rightarrow Bi + 3F^-$) proceeds in CsF(sat.)-TPhBX(0.50)-G4. Furthermore, the electrolyte partially decomposed, and the decomposition product was formed on the particles of active material. From the fully discharged to fully charged states, the intensity of peaks assigned to Bi metal decreased while that assigned to BiF_3 increased. This indicates that the charge reaction ($Bi + 3F^- \rightarrow BiF_3 + 3e^-$) proceeds in CsF(sat.)-TPhBX(0.50)-G4.

The XPS results indicate that the discharge and charge reactions proceed in both electrolytes. Conversely, the progress of electrolyte decomposition during discharging is observed only in CsF(sat.)-TPhBX(0.50)-G4.

3.4. Amount of dissolved Bi during discharging and charging in each electrolyte

The XPS results confirmed the formation of Bi and BiF_3 during discharging and charging with both electrolytes. Herein, we believed that the side reaction caused the differences in the cycling performance between the two electrolytes as shown in Figure 2. It was reported that the addition of AA increased the solubility of both BiF_3 and CsF. [15] Furthermore, the dissolution of active material during charging was observed when using the electrolyte comprised G4, CsF (0.45 mol dm^{-3}), and FBTMPhB (0.50 mol dm^{-3}), and the amount of dissolved active material was reduced by an increase in the CsF/FBTMPhB ratio in the electrolyte. [16] Thus, we attributed the difference in the cycling performances of the electrolytes to the difference in the amount of dissolved active material.

We expected that the difference in the dissolved active material might cause the difference in the cycling performance in electrolytes containing different CsF/TPhBX ratios. The amount of dissolved active material in each electrolyte was investigated using AAS. The amount of dissolved Bi in the fully charged and discharged states prepared using each electrolyte is summarized in Table 1. The amounts of dissolved Bi in the fully discharged and charged states prepared using CsF(0.45)-TPhBX(0.50)-G4 were 0.08% and 37%, respectively. Conversely, the amounts of dissolved Bi in the fully discharged

and charged states prepared using CsF(sat.)-TPhBX(0.50)-G4 were < 0.02% and 0.2%, respectively. The amount of dissolved Bi in CsF(0.45)-TPhBX(0.50)-G4 increased considerably from the fully discharged state to the fully charged state, indicating that dissolution of Bi ($Bi \rightarrow Bi^{3+} + 3e^{-}$) occurs during charging. The dissolution of Bi results in loss of active material, which causes capacity degradation. Conversely, the amount of dissolved Bi in CsF(sat.)-TPhBX(0.50)-G4 hardly changed from the fully discharged state to the fully charged state, indicating that dissolution of active material hardly occurs during charging. Thus, the capacity reduction in CsF(0.45)-TPhBX(0.50)-G4 is mainly attributed to loss of active material due to Bi dissolution during charging. Furthermore, the dissolution of 37% Bi during charging when using CsF(0.45)-TPhBX(0.50)-G4 indicates that the charge capacity of 112 mAh g^{-1} was obtained by the dissolution of Bi ($Bi \rightarrow Bi^{3+} + 3e^{-}$). Thus, the increase in the peak intensity assigned to Bi^{3+} in the XPS (Figure 3(a)) was attributed to BiF_3 formation; however, the decrease in the peak intensity assigned to Bi was mainly attributed to Bi loss due to dissolution. Conversely, BiF_3 formation mainly occurs during charging when using CsF(sat.)-TPhBX(0.50)-G4.

3.5. Particle configuration and elemental distributions of Bi and F in the active material during discharging

From the XPS results (Figure 3), the decomposition product of the electrolyte was observed only when using CsF(sat.)-TPhBX(0.50)-G4. Furthermore, from the AAS results (Table 1), the amount of dissolved Bi in each electrolyte was different. We therefore expected that the solubility of Bi and/or electrolyte decomposition might affect Bi formation during discharging in each electrolyte.

To evaluate the formation state of Bi during discharging, the particle configurations and elemental distributions of a cross-section of the electrode prepared with both electrolytes were investigated using SEM/EDX. Backscattered electron (BE) images and Bi and F EDX maps of a cross-section of an electrode in the pristine state are shown in Figure 4. In Figure 4(a), the bright structure in the center of the image is assigned to BiF_3, because Bi and F were detected in this area by EDX mapping (Figure 4(b) and (c)).

A BE image, and Bi and F EDX maps of a cross-section of electrode in partially discharged states (151 mAh g^{-1}) prepared using CsF(0.45)-TPhBX(0.50)-G4 are shown in Figure 5. In Figure 5(a), the bright structure in the center of the image is indexed to the active material because Bi was detected in this area by the EDX mapping (Figure 5(b)). In the BE image, the upper and left lower areas of the active material were brighter than the other areas (Figure 5(a)). Also in the BE image, the average atomic number of the

light area is larger than that of the dark area. In Figure 5(c), the area in which F was detected corresponded to the darker area of the active material in the BE image (Figure 5(a)). EDX mapping indicate that Bi and BiF_3 exist in the bright and dark areas of the active material shown in Figure 5(a), respectively. This corresponds to the contrast in the BE image (Figure 5(a)).

When using CsF(sat.)-TPhBX(0.50)-G4, the decomposition product of the electrolyte was confirmed by XPS analysis (Figure 3(b)); therefore, the elemental distributions of O and Cs were also evaluated. A BE image, and Bi, F, O, and Cs EDX maps of a cross-section of the electrode in the partially discharged states (151 mAh g^{-1}) prepared using CsF(sat.)-TPhBX(0.50)-G4 are shown in Figure 6. In Figure 6(a), the bright structure in the center of the image is indexed to the active material because Bi was detected in this area by EDX mapping (Figure 6(b)). White and gray areas were observed in the active material, and the gray area is surrounded by a white area (Figure 6(a)). As shown in Figure 6(c), F was detected in the gray area in Figure 6(a). This indicates that Bi exists around the surface of BiF_3 prepared using CsF(sat.)-TPhBX(0.50)-G4. Furthermore, as shown in Figure 6(c), F was also detected in the dark gray area around the active material (Figure 6(a)). As shown in Figure 6(d) and (e), the locations where O and Cs were detected corresponded to the dark gray area in Figure 6(a). These results

indicate that an electrolyte decomposition product comprising F, O, and Cs existed around the active material when using CsF(sat.)-TPhBX(0.50)-G4. As shown in Figure 2, the potential of the first discharge reaction for BiF_3 electrode was lowered by the change of electrolyte composition from CsF(0.45)-TPhBX(0.5)-G4 to CsF(sat.)-TPhBX(0.50)-G4. Due to the lower reaction potential, the electrolyte decomposition product was formed in case of using CsF(sat.)-TPhBX(0.50)-G4.

The SEM/EDX analysis indicate that Bi formation was proceeded during discharging when using both electrolytes. As shown in Figure 5(a), when BiF_3 electrode was discharged using CsF(0.45)-TPhBX(0.50)-G4, Bi was formed in the upper and left lower areas (white area of active material) of the BiF_3 particle (gray area of the active material). As shown in Figure 6(a), when BiF_3 electrode was discharged using CsF(sat.)-TPhBX(0.50)-G4, Bi was formed surrounding area (white area of active material) of the BiF_3 particle (gray area of active material). These results indicate that the formation state of Bi was affected by the electrolyte. The electronic conductivity of metallic Bi is higher than that of BiF_3; therefore, the formation of Bi during discharging was proceeded around Bi. This enhances the growth of a Bi domain or the formation of Bi shell structure in the active material particle. However, the state of Bi in each electrolyte was different.

As shown in Table 1, the high amount of dissolving Bi was detected in the

electrolyte (CsF(0.45)-TPhBX(0.50)-G4) after charging; however, the little dissolved Bi was detected after discharging. These indicate that Bi was lost from the electrode to electrolyte and Bi existed in the electrode after charging and discharging, respectively. Also, Bi on BiF_3 particles were observed in the cross-sectional SEM image after discharging (Figure 5(a)). Therefore, we concluded that during discharging, dissolved Bi in the electrolyte was deposited on the electrode. Because Bi can be deposited on any sites in the electrode contacted with electrolyte, the deposited Bi was observed in the many different areas (Figure 5(a)). Conversely, the BiF_3 hardly dissolved in CsF(sat.)-TPhBX(0.50)-G4; therefore, Bi formation was progressed from the BiF_3 surface. Furthermore, a surface film comprising F, O, and Cs formed around the active material particles when using CsF(sat.)-TPhBX(0.50)-G4. The change in the state of Bi and/or the surface film lowered the discharge reaction potential. The CsF/TPhBX ratio affects Bi dissolution during charging, and the state of Bi and electrolyte decomposition during discharging. Differences in the discharge and charge reaction mechanism cause differences in electrochemical properties such as cycling performance and the potentials of the discharge and charge reactions.

Conclusions

The effect of the CsF/TPhBX ratio in the electrolyte on the electrochemical performance of BiF_3 electrode was investigated using CsF(0.45)-TPhBX(0.50)-G4 and CsF(sat.)-TPhBX(0.50)-G4 as electrolytes. The discharge and charge reactions of BiF_3 electrodes proceeded in both electrolytes; however, the electrochemical properties of electrodes differ between the two electrolytes. The XPS results indicate that Bi and BiF_3 were formed during discharging and charging, respectively, regardless of the CsF/TPhBX ratio in the electrolyte. The AAS results indicate that the dissolution of Bi during charging when using CsF(0.45)-TPhBX(0.50)-G4 caused the differences in the cycling performance compared with those when using CsF(sat.)-TPhBX(0.50)-G4. The SEM/EDX results indicate that the progress of discharge reaction was confirmed in both electrolytes; however, the formation state of Bi and progress of electrolyte decomposition differed between the two electrolytes. The discharge and charge reactions of BiF_3 proceeded using the electrolyte comprising G4, CsF, and TPhBX; however, the electrochemical reaction mechanism and electrochemical properties were dependent on the CsF/TPhBX ratio in the electrolyte.

Acknowledgment section

This work was supported by the Research and Development Initiative for Scientific Innovation of New Generation Batteries (RISING) and Research and Development Initiative for Scientific Innovation of New Generation Batteries 2 (RISING2) projects from the New Energy and Industrial Technology Development Organization (NEDO), Japan. The authors thank Ms. Kiyomi Ishizawa, Ms. Ryoko Masuda, and Ms. Hisayo Ikeda for their experimental support.

References

(1) Nishi, Y.; Lithium Ion Secondary Batteries; Past 10 Years and the Future, *J. Power Sources* 2001, 100, 101–106.

(2) Wang, Y.; Liu, B.; Li, Q.; Cartmell, S.; Ferrara, S.; Deng, Z. D.; Xiao, J.; Lithium and Lithium Ion Batteries for Applications in Microelectronic Devices: A review, *J. Power Sources* 2015, 286, 330–345.

(3) Minato, T.; Abe, T.; Surface and Interface Sciences of Li-ion Batteries –Research Progress in Electrode-electrolyte Interface–, *Prog. Surf. Sci.* 2017, 92, 240–280.

(4) Delmas, C.; Braconnier, J. J.; Fouassier, C.; Hagenmuller, P.; Electrochemical Intercalation of Sodium in Na_xCoO_2 Bronzes, *Solid State Ion.* 1981, 3–4, 165–169.

(5) Aurbach, D.; Lu, Z.; Schechter, A.; Gofer, Y.; Gizbar, H.; Turgeman, R.; Cohen, Y.; Moshkovich, M.; Levi, E.; Prototype Systems for Rechargeable Magnesium Batteries, *Nature* 2000, 407, 724–727.

(6) Eftekhari, A.; Potassium Secondary Cell Based on Prussian Blue Cathode, *J. Power Sources* 2004, 126, 221–228.

(7) Abraham, K. M.; Jiang, Z.; A Polymer Electrolyte-Based Rechargeable Lithium/Oxygen Battery, *J. Electrochem. Soc.* 1996, 143, 1–5.

(8) Reddy, M. A.; Fichtner, M; Batteries Based on Fluoride Shuttle, *J. Mater. Chem.* 2011,

21, 17059–17062.

(9) Rongeat, C.; Reddy, M. A.; Witter, R.; Fichtner, M.; Nanostructured Fluoride-Type Fluorides As Electrolytes for Fluoride Ion Batteries, *J. Phys. Chem. C* 2013, 117, 4943–4950.

(10) Gschwind, F.; Zhao-Karger, Z.; Fichtner, M.; A Fluoride-doped PEG Matrix as an Electrolyte for Anion Transportation in a Room-temperature Fluoride Ion Battery, *J. Mater. Chem. A* 2014, 2, 1214–1218.

(11) Gschwind, F.; Bastien, J.; Parametric Investigation of Room-temperature Fluoride-ion Batteries: Assessment of Electrolytes, Mg-based Anodes, and BiF_3-cathodes, *J. Mater. Chem. A* 2015, 3, 5628–5634.

(12) Grenier, A.; Porras-Gutierrez, A.; Groult, H.; Beyer, K. A.; Borkiewicz, O. J.; Chapman, K. W.; Dambournet, D.; Electrochemical Reactions in Fluoride-ion Batteries: Mechanistic Insights from Pair Distribution Function Analysis, *J. Mater. Chem. A* 2017, 5, 15700–15705.

(13) Nowroozi, M. A.; Wissel, K.; Rohrer, J.; Munnangi, A. R.; Clemens, O.; $LaSrMnO_4$: Reversible Electrochemical Intercalation of Fluoride Ions in the Context of Fluoride Ion Batteries, *Chem. Mater.* 2017, 29, 3441–3453.

(14) Davis, V. K.; Bates, C. M.; Omichi, K.; Savoie, B. M.; Momcilovic, N.; Xu, Q.; Wolf,

W. J.; Webb, M. A.; Billings, K. J.; Chou, N. H. et al; Room-temperature Cycling of Metal Fluoride Electrodes: Liquid Electrolytes for High-energy Fluoride Ion Cells, *Science* 2018, 362, 1144–1148.

(15) Konishi, H; Minato, T; Abe, T; Ogumi, Z.; Electrochemical Performance of a Bismuth Fluoride Electrode in a Reserve-Type Fluoride Shuttle Battery, *J. Electrochem. Soc.* 2017, 164, A3702–A3708.

(16) Konishi, H; Minato, T; Abe, T; Ogumi, Z.; Improvement of Cycling Performance in Bismuth Fluoride Electrodes by Controlling Electrolyte Composition in Fluoride Shuttle Batteries, *J. Appl. Electrochem.* 2018, 48, 1205–1211.

(17) Konishi, H; Minato, T; Abe, T; Ogumi, Z.; Electrochemical Properties of Lead Fluoride Electrode in Fluoride Shuttle Battery, *J. Electroanal. Chem.* 2018, 826, 60–64.

(18) Konishi, H; Minato, T; Abe, T; Ogumi, Z.; Triphenylboroxine and Triphenylborane as Anion Acceptors for Electrolyte in Fluoride Shuttle Batteries, *Chem. Lett.* 2018, 47, 1346–1349.

(19) Lee, H. S.; Yang, X. Q.; Xiang, C. L.; McBreen, J.; The Synthesis of a New Family of Boron-Based Anion Receptors and the Study of Their Effect on Ion Pair Dissociation and Conductivity of Lithium Salts in Nonaqueous Solutions, *J. Electrochem. Soc.* 1998, 145, 2813–2818.

(20) Lee, H. S.; Sun, X.; Yang, X. Q.; McBreen, J.; Synthesis and Study of New Cyclic Boronate Additives for Lithium Battery Electrolyte, *J. Electrochem. Soc.* 2002, 149, A1460–A1465.

(21) Li, L. F.; Lee, H. S.; Li, H.; Yang, X. Q.; Nam, K. W.; Yoon, W. S.; McBreen, J.; Huang, X. J.; New Electrolytes for Lithium Ion Batteries Using LiF Salt and Boron Based Anion Receptors, *J. Power Sources* 2008, 184, 517–521.

(22) Xie, B.; Lee, H. S.; Li, H.; Yang, X. Q.; McBreen. J; Chen, L. Q.; New Electrolytes Using Li_2O or Li_2O_2 Oxides and Tris(pentafluorophenyl)borane as Boron Based Anion Receptor for Lithium Batteries, *Electrochem. Commun.* 2008, 10, 1195–1197.

(23) Chen, Z.; Amine, K.; Computational Estimates of Fluoride Affinity of Boron-Based Anion Receptors, *J. Electrochem. Soc.* 2009, 156, A672–A676.

(24) Bervas, M.; Badway, F., Klein, L. C.; Amatucci, G. G.; Bismuth Fluoride Nanocomposite as a Positive Electrode Material for Rechargeable Lithium Batteries, *Electrochem Solid-State Lett.* 2005, 8, A179–A183.

(25) Bervas, M; Mansour, A. N.; Yoon, W. S.; Al-Sharab, J. F.; Badway, F.; Cosandey, F; Klein, L. C.; Amatucci, G. G.; Investigation of the Lithium and Delithiation Conversion Mechanisms of Bismuth Fluoride Nanocomposites, *J. Electrochem. Soc.* 2006, 153, A799–A808.

(26) Gmitter, A. J.; Badway, F.; Rangan, S., Bartynski, R. A.; Halajko, A.; Pereira, N.; Amatucci, G. G.; Formation, Dynamics, and Implication of Solid Electrolyte Interface in High Voltage Reversible Conversion Fluoride Nanocomposites, *J. Mater. Chem.* 2010, 20, 4149–4161.

(27) Konishi, H; Minato, T; Abe, T; Ogumi, Z.; Cycling Fading Mechanism for a Bismuth Fluoride Electrode in a Lithium-Ion Battery, *Chemistry Select* 2017, 2, 3504–3510.

(28) Konishi, H; Minato, T; Abe, T; Ogumi, Z.; Electrochemical Reaction Mechanism for $Bi_{1-x}Ba_xF_{3-x}$ (x = 0, 0.1, 0.2, and 0.4) Electrodes in Lithium-Ion Batteries, *Chemistry Select* 2017, 2, 6399–6406.

(29) Konishi, H; Minato, T; Abe, T; Ogumi, Z.; Difference of Rate Performance between Discharge and Charge Reactions for Bismuth Fluoride Electrode in Lithium-ion Battery, *J. Electroanal. Chem.* 2017, 806, 82–87

(30) Pavlishchuk, V. V.; Addison, A. W.; Inorg. Conversion Constants for Redox Potentials Measured versus Different Reference Electrodes in Acetonitrile Solutions at 25°C, *Chim. Acta* 2000, 298, 97–102.

(31) Morgan, W. E.; Stec, W. J.; Van Wazer, J. R.; Inner-Orbital Binding-Energy Shifts of Antimony and Bismuth Compounds, *Inorg. Chem.* 1973, 12, 953–955.

(32) Gmitter, A. J.; Halajko, A.; Sideris, P. J.; Greenbaum, S. G.; Amatucci, G. G.,

Subsurface Diffusion of Oxide Electrolyte Decomposition Products in Metal Fluoride Nanocomposite Electrodes, *Electrochim. Acta*, 2013, 88, 735–744.

(33) Iranmahboob, J.; Toghiani, H.; Hill, D. O.; Dispersion of Alkali on the Surface of C0-MoS_2/clay Catalyst: a Comparison of K and Cs as a Promotor for Synthesis of Alcohol, *Appl. Catal. A.: Gen.* 2003, 247, 207–218.

Author contributions

H. Konishi and T. Minato designed and performed the experiments. All authors discussed the experiment results. H. Konishi and T. Minato wrote the manuscript, and all authors have given approval to the final version of the manuscript.

Figure and table captions

Figure 1. Cyclic voltammograms of a Pt electrode in CsF(0.45)-TPhBX(0.50)-G4 and CsF(sat.)-TPhBX(0.50)-G4 within potential range from –3.0 to 0 V (vs. ref.).

Figure 2. Discharge and charge curves of BiF_3 in CsF(sat.)-TPhBX(0.50)-G4 from –2.0 to –0.2 V (vs. ref.) during the first, second, and third cycles. [Insert: discharge and charge curves of BiF_3 in CsF(0.45)-TPhBX(0.50)-G4 from –1.2 to –0.2 V (vs. ref.) during the first, second, and third cycles. These were reproduced using the data from ref.[18]]

Figure 3. Bi 4f XPS spectra of the BiF_3 electrode in the pristine, partially discharged (151 mAh g^{-1}), fully discharged, and fully charged states prepared in (a) CsF(0.45)-TPhBX(0.50)-G4 and (b) CsF(sat.)-TPhBX(0.50)-G4.

Figure 4. SEM images and EDX maps for BiF_3 in the pristine state [(a) SEM (backscattered electron image), (b) EDX map: Bi, and (c) EDX map: F].

Figure 5. SEM images and EDX maps for BiF_3 in the partially discharged state (151 mAh g^{-1}) prepared in CsF(0.45)-TPhBX(0.50)-G4 [(a) SEM (backscattered electron

image), (b) EDX map: Bi, and (c) EDX map: F].

Figure 6. SEM images and EDX maps for BiF_3 in the partially discharged state (151 mAh g^{-1}) prepared in CsF(sat.)-TPhBX(0.50)-G4 [(a) SEM (backscattered electron image), (b) EDX map: Bi, (c) EDX map: F, (d) EDX map: O, and (e) EDX map: Cs].

Table 1. Amount of dissolved Bi in the fully discharged and charged states prepared in CsF(0.45)-TPhBX(0.50)-G4 and CsF(sat.)-TPhBX(0.50)-G4.

Figures, Tables

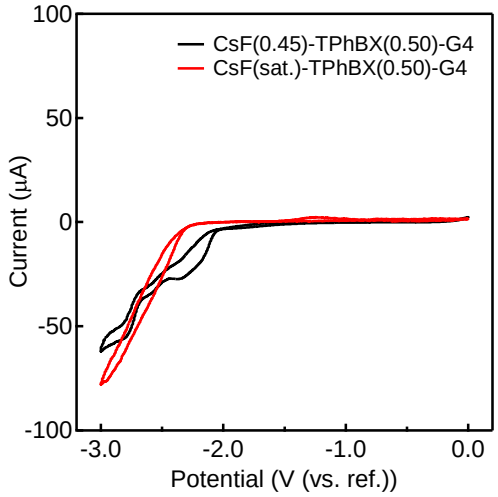

Figure 1. Cyclic voltammograms of a Pt electrode in CsF(0.45)-TPhBX(0.50)-G4 and CsF(sat.)-TPhBX(0.50)-G4 within potential range from –3.0 to 0 V (vs. ref.).

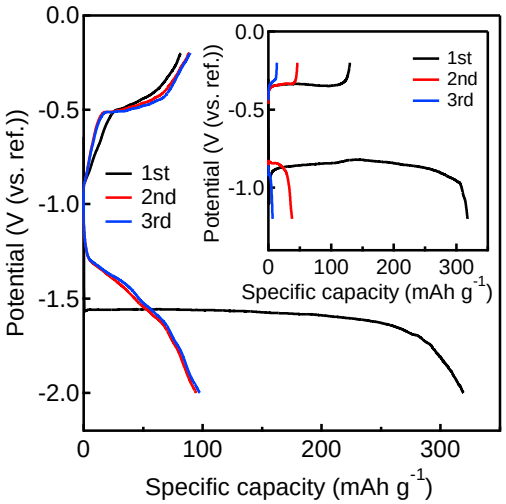

Figure 2. Discharge and charge curves of BiF_3 in CsF(sat.)-TPhBX(0.50)-G4 from –2.0 to –0.2 V (vs. ref.) during the first, second, and third cycles. [Insert: Discharge and charge curves of BiF_3 in CsF(0.45)-TPhBX(0.50)-G4 from –1.2 to –0.2 V (vs. ref.) during the first, second, and third cycles. These were reproduced using the data from ref.[18]]

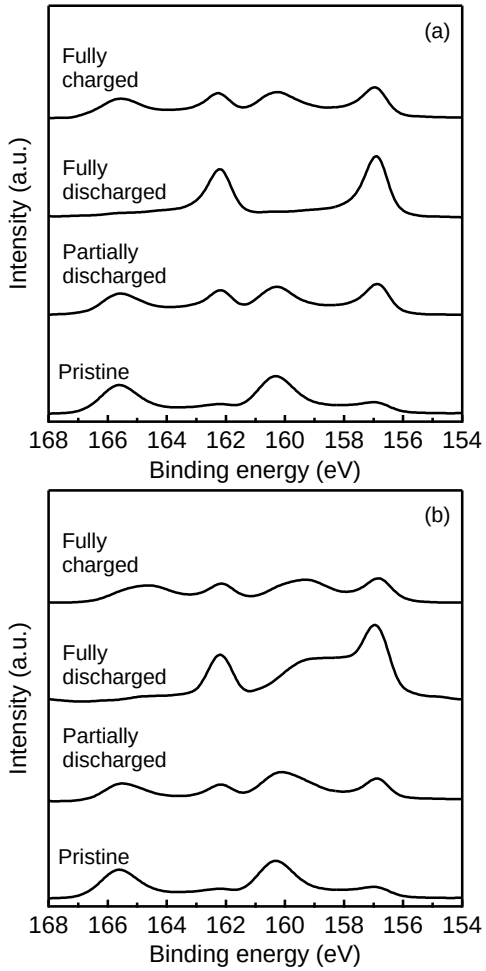

Figure 3. Bi 4f XPS spectra of the BiF_3 electrode in the pristine, partially discharged (151 mAh g^{-1}), fully discharged, and fully charged states prepared in (a) CsF(0.45)-TPhBX(0.50)-G4 and (b) CsF(sat.)-TPhBX(0.50)-G4.

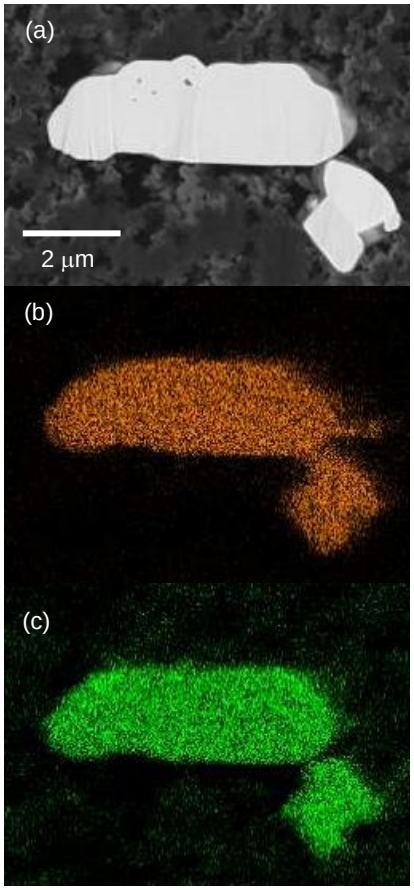

Figure 4. SEM images and EDX maps for BiF_3 in the pristine state [(a) SEM (backscattered electron image), (b) EDX map: Bi, and (c) EDX map: F].

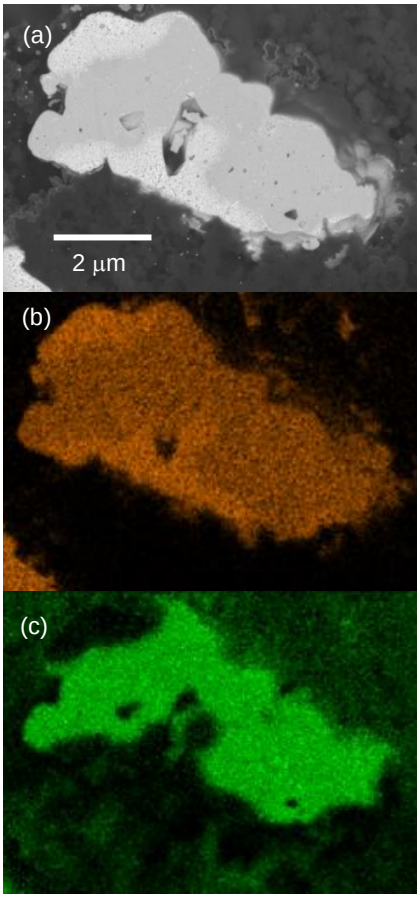

Figure 5. SEM images and EDX maps for BiF_3 in the partially discharged state (151 mAh g^{-1}) prepared in CsF(0.45)-TPhBX(0.50)-G4 [(a) SEM (backscattered electron image), (b) EDX map: Bi, and (c) EDX map: F].

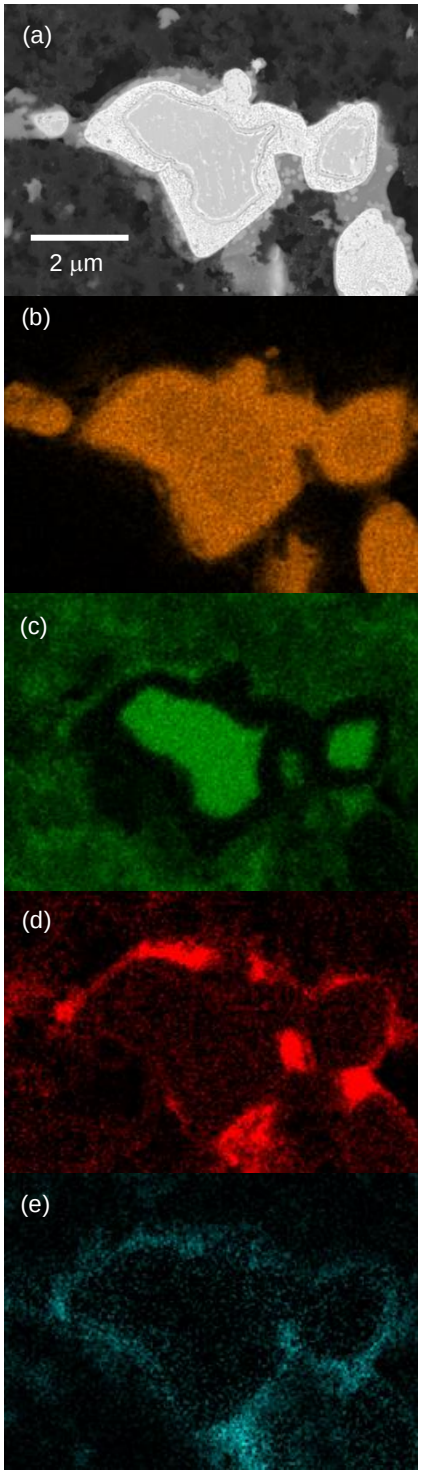

Figure 6. SEM images and EDX maps for BiF_3 in the partially discharged state (151 mAh g^{-1}) prepared in CsF(sat.)-TPhBX(0.50)-G4 [(a) SEM (backscattered electron image), (b) EDX map: Bi, (c) EDX map: F, (d) EDX map: O, and (e) EDX map: Cs].

Table 1. Amount of dissolved Bi in the fully discharged and charged states prepared in CsF(0.45)-TPhBX(0.50)-G4 and CsF(sat.)-TPhBX(0.50)-G4.

	Amount of dissolved Bi (%)	
Electrolyte	Discharge	Charge
CsF(0.45)-TPhBX(0.5)-G4	0.08	37
CsF(sat.)-TPhBX(0.5)-G4	< 0.02	0.2

TOC Graphic

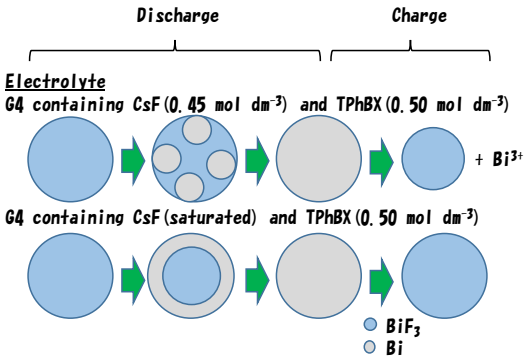
Discharge
Charge
Electrolyte
G4 containing CsF (0.45 mol dm-3) and TPhBX (0.50 mol dm-3)
+ Bi3+
G4 containing CsF (saturated) and TPhBX (0.50 mol dm-3)
BiF3
Bi